nature neuroscience

# Functional imaging of hippocampal place cells at cellular resolution during virtual navigation

Daniel A Dombeck[1], Christopher D Harvey[1], Lin Tian[2], Loren L Looger[2] & David W Tank[1]

**Spatial navigation is often used as a behavioral task in studies of the neuronal circuits that underlie cognition, learning and memory in rodents. The combination of *in vivo* microscopy with genetically encoded indicators has provided an important new tool for studying neuronal circuits, but has been technically difficult to apply during navigation. Here we describe methods for imaging the activity of neurons in the CA1 region of the hippocampus with subcellular resolution in behaving mice. Neurons that expressed the genetically encoded calcium indicator GCaMP3 were imaged through a chronic hippocampal window. Head-restrained mice performed spatial behaviors in a setup combining a virtual reality system and a custom-built two-photon microscope. We optically identified populations of place cells and determined the correlation between the location of their place fields in the virtual environment and their anatomical location in the local circuit. The combination of virtual reality and high-resolution functional imaging should allow a new generation of studies to investigate neuronal circuit dynamics during behavior.**



The location-specific firing of hippocampal place cells[1] during navigation represents a salient neural correlate of spatial information in the mammalian brain. More generally, place cells and other hippocampal neurons are thought to be involved in the encoding of episodic memories[2], making the behaving animal the most appropriate setting in which to study their activity patterns. The firing properties of hippocampal neurons in behaving rodents have been characterized using extracellular electrode techniques in numerous experimental paradigms[3,4]. However, electrophysiological methods have limitations in characterizing precise spatio-temporal activity patterns, targeting genetically labeled subpopulations and monitoring subcellular compartments.

For example, it is unclear whether hippocampal neurons with similar place fields are spatially organized within the hippocampus. Although some studies have reported organization on spatial scales ranging from tens of micrometers[5] to millimeters[6,7], a separate study found no organization on either of these scales[8]. This question has been difficult to address because extracellular electrodes cannot report the precise anatomical location of the recorded cells[6–9]. Indirect methods, such as immediate early gene (IEG) expression[5,8], are also problematic because the relationship between gene expression and neuronal spiking is not well established. Tetrode recordings have revealed no correlation between place field location and a cell's anatomical location[8]. By contrast, IEG studies have provided evidence for micro-clustering of cells that were active in restricted places within a larger environment[5].

Optical imaging of neuronal activity at a high spatial resolution can address these and other questions by providing a full spatio-temporal view of neuronal population activity within a microcircuit, by recording from genetically labeled neuronal subtypes, and by monitoring subcellular compartments such as dendritic branches and spines. However, it is not currently possible to perform high-resolution functional imaging of neurons in the hippocampi of awake, navigating mice. To achieve this goal, three obstacles must be overcome: cellular resolution imaging in the brain of a mobile mouse; imaging more than a millimeter beneath the cortical surface; and imaging that is compatible with navigation behavior. Two-photon microscopy[10] in combination with calcium-sensitive dyes has been used to provide cellular resolution functional imaging in awake mobile mice on a spherical treadmill[11,12]. Chronic functional imaging in this preparation has been made possible using the genetically encoded calcium indicator GCaMP3[13]. In an acute anesthetized mouse preparation, non-activity dependent fluorescent probes have been used for subcellular imaging of the hippocampus[14]. In addition, a virtual reality system has been developed that allows spatial behaviors to be studied in head-restrained mice[15].

Here, we combined and extended these methods to make possible high-resolution functional imaging of the hippocampus in mice navigating in a virtual reality environment. We developed a preparation for chronic imaging of CA1 neuronal activity with cellular and subcellular resolution in awake mice with their heads restrained while they ran on a spherical treadmill. This was combined with a custom two-photon microscope and light-blocking methods designed for imaging in the presence of the visual display surrounding the treadmill that defined a virtual environment. Using these methods, we optically recorded from populations of ~80–100 GCaMP3-expressing neurons in the CA1 region of the hippocampus while the mouse was running along a linear track. Subpopulations of the recorded neurons were identified as place cells. Because our methods could precisely determine the physical location of the place cells in the hippocampus, we could show that for cells separated by more than a few tens of micrometers, there was no strong relationship in our experimental paradigm between the location of place fields in the virtual reality environment and the position of the corresponding place cells in area CA1. Nearby cells

[1]Department of Molecular Biology and Princeton Neuroscience Institute, Princeton University, Princeton, New Jersey, USA. [2]Howard Hughes Medical Institute, Janelia Farm Research Campus, Ashburn, Virginia, USA. Correspondence should be addressed to D.W.T. (dwtank@princeton.edu) or D.A.D. (ddombeck@princeton.edu).

Received 3 May; accepted 1 September; published online 3 October 2010; doi:10.1038/nn.2648

(less than <35 μm separation) showed enhanced correlation, although the possibility that this was produced by mixing of optical signals from adjacent cells could not be excluded. In addition, we show that it is possible to record place-related activity in putative hippocampal interneurons and CA1 apical dendrites.

## RESULTS

### Combining two-photon microscopy and mouse virtual reality

Our apparatus (**Fig. 1a**,**b**) was designed around our previously described virtual reality system[15]. The limbs of a head-restrained mouse rested on a spherical treadmill[12]. A toroidal screen that subtended a mouse's visual field surrounded the treadmill and displayed a computer-generated image of a virtual environment[15,16]. Ball movements recorded with an optical computer mouse provided information on running speed and direction and this was used by the computer program that implemented the virtual environment to update position and view angle. As reported previously[15], head-restrained mice were trained using operant conditioning to run back and forth along a 180 cm–long virtual linear track (**Fig. 1c**). The mice received water rewards at the ends of the track after successfully traversing the full track length; consecutive rewards at the same end were not available.

We designed and constructed a two-photon microscope that could fit within the geometric constraints of our virtual reality apparatus without obstructing the mouse's view of the display (**Fig. 1a**). The physical dimensions of the design were most severely constrained by the small distance (~13 cm) between the top of the headplate on the mouse's head and the bottom of the reflecting mirror in the virtual reality projection path. In addition, we designed the microscope to be completely shielded from the bright light of the virtual reality projection display so that the smaller number of photons from the fluorescent probe could be detected by the photomultiplier tubes (PMTs) without contamination. We then implemented additional light-blocking measures at the laser input port and the hole for the microscope objective (see Online Methods; **Fig. 1a**,**d**,**e**) so that the amount of detected background light was less than ~5% of the baseline fluorescence level from labeled cells.

### A window for chronic imaging of CA1 neurons in awake mice

The CA1 region of the hippocampus is more than a millimeter below the cortical surface and cannot be directly imaged using two-photon microscopy[17]. We carefully removed the overlying cortex by aspiration (down to the external capsule) and replaced it with a metal cannula with a coverslip sealing one of the openings (see Online Methods, **Fig. 1e**). This created a chronic hippocampal window that allowed direct imaging of the hippocampus.

We used genetically encoded calcium indicators to optically record the activity of CA1 neurons. Hippocampal injections of adeno-associated virus AAV2/1-*synapsin-1*-GCaMP3 (a moderate, neuron-specific promoter[18] in a serotype with efficient gene delivery to neurons[19]) resulted in expression of GCaMP3 in a large population of CA1 neurons. Two-photon imaging of the GCaMP3-expressing area at a shallow depth through the hippocampal window showed axons in the external capsule and alveus that appeared as a dense plexus of fibers running parallel to the hippocampal surface (**Fig. 1f**). Inspection of images from the stratum pyramidale (~130–160 μm below the external capsule) revealed the densely packed neurons of this cell body layer. We did not see voids of fluorescence indicative of unlabeled cells, suggesting that local labeling was nearly ubiquitous (**Fig. 1f**; note that GCaMP3 is excluded from the nucleus, which causes a 'donut-like' appearance of the cell bodies[13]). All pyramidal neuron cell bodies in the stratum pyramidale have a prominent apical dendrite that projects ventrally into the stratum radiatum (deeper into the hippocampus). Imaging perpendicular to the long axis of these dendrites in the stratum radiatum showed their cross-sections as small dots (**Fig. 1f**; see **Supplementary Movie 1** for a *z*-series through the labeled CA1 region).

### Optical identification of CA1 place cells

We developed a timeline for the sequence of steps necessary to image hippocampal activity in mice trained to perform the spatial behavior

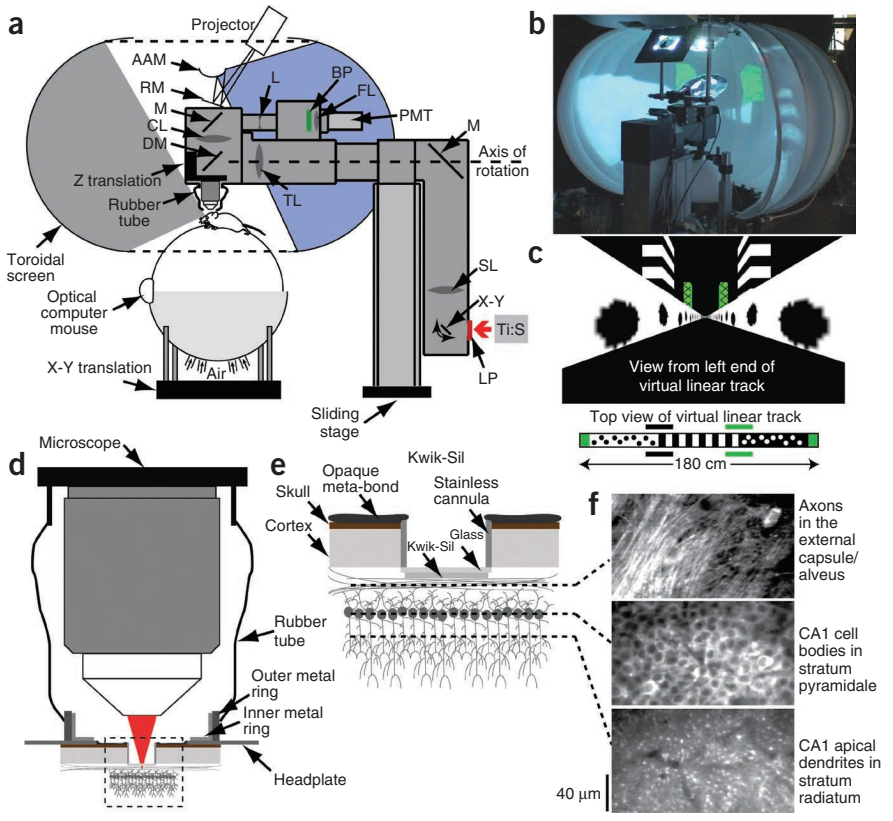


**Figure 1** Experimental setup. (**a**) The experimental apparatus, consisting of a spherical treadmill, a virtual reality apparatus (projector, reflecting mirror (RM), angular amplification mirror (AAM), toroidal screen and optical computer mouse to record ball rotation) and a custom two-photon microscope (titanium: sapphire laser (Ti:S), long-pass filter (LP), galvanometers (X-Y), scan lens (SL), mirror (M), tube lens (TL), dichroic mirror (DM), collection lens (CL), biconcave lens (L), bandpass filter (BP), focusing lens (FL), photomultiplier tube (PMT), sliding stage (used to move microscope for treadmill access), X-Y translation (moves treadmill and mouse), Z-translation (objective focus control) and rubber tube (shown in cross-section, for light shielding)). (**b**) Photograph of experimental setup. (**c**) Top, view from one end of the virtual linear track. Bottom, top view of the linear track. (**d**) View of materials used to block background light from entering the microscope objective hole. Hippocampal imaging window can also be seen. (**e**) Detailed view of hippocampal imaging window (from boxed region in **d**). (**f**) *In vivo* two-photon images at different depths through the hippocampal window.

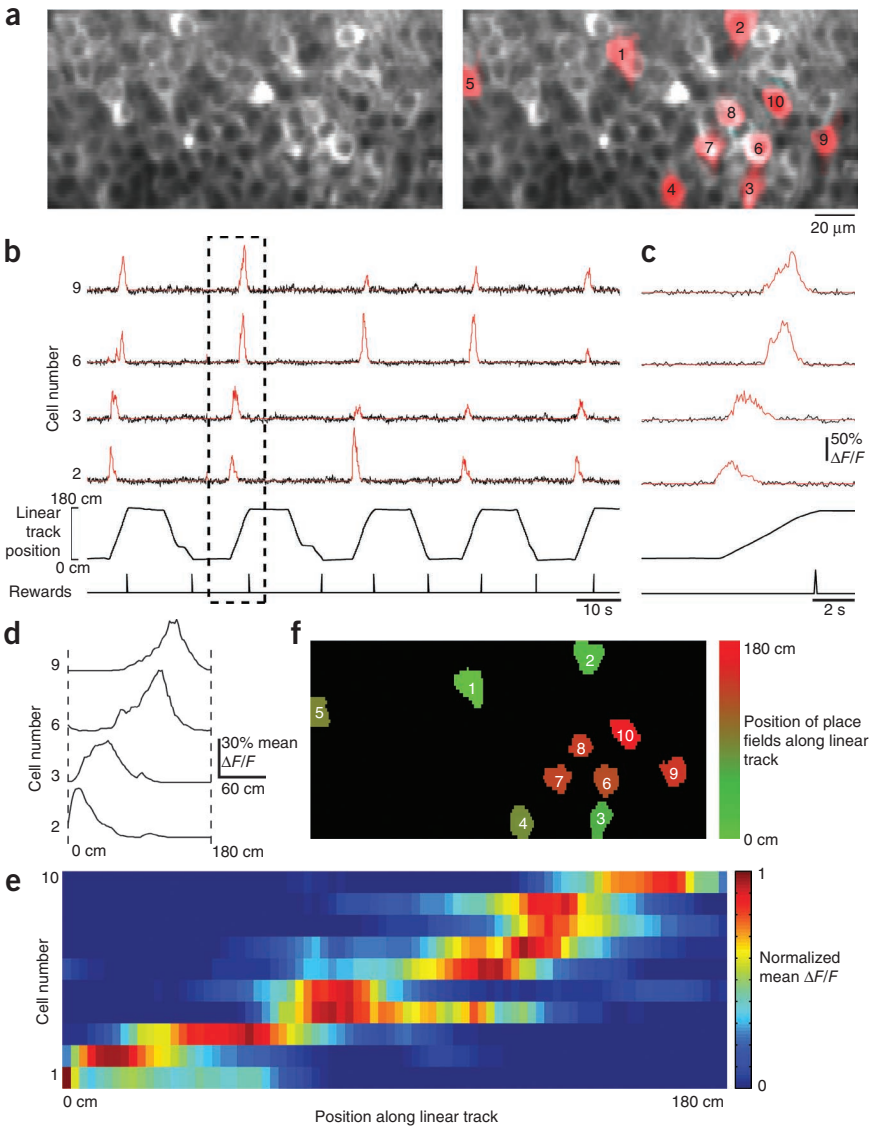


**Figure 2** Imaging CA1 place cells in the dorsal hippocampus. (**a**) Two-photon image of neuron cell bodies in stratum pyramidale of CA1 labeled with GCaMP3. The indicator is excluded from the nucleus[13]. ROIs for example cells are shown in red (right). (**b**) GCaMP3 baseline subtracted $\Delta F/F$ traces are shown in black for a subset of the cells labeled in **a** (right). Red traces indicate significant calcium transients with <5% false positive error rates (see Online Methods). The position of the mouse along the virtual linear track and reward times are shown at the bottom. (**c**) Expanded view of boxed region in **b**. (**d**) Mean $\Delta F/F$ versus linear track position for a subset of the cells labeled in **a** (right). (**e**) A plot of mean $\Delta F/F$ versus linear track position for all of the cells labeled in **a** (right). (**f**) Place cells are colored according to the location of their place fields along the virtual linear track. Only place cells with significant place fields during running in the positive direction are shown.

task. Mice were first implanted with a metal headplate to allow their heads to be restrained while they were on the spherical treadmill. They were placed on water scheduling for several days and then trained in the virtual reality apparatus. Once the mice were proficient at the task (~2 rewards per minute, ~7–10 d of training) we injected the GCaMP3 virus, and the next day we implanted the hippocampal window. The mice were returned to behavioral training for ~5–7 d until the GCaMP3 expression produced an acceptable signal-to-noise ratio for imaging calcium transients. Using the hippocampal imaging window and viral delivery of GCaMP3, we could image activity in CA1 neurons repeatedly over the course of about 3–4 weeks.

To optically identify and characterize place cells, we collected time-series movies (~64 ms per frame) of fields of view (~200 × 100 μm) in the CA1 region of the hippocampus containing ~80–100 neurons (**Fig. 2a**) while the mice navigated the virtual linear track. We acquired time series at a single location in CA1 for ~9–13 min. In all, we analyzed 47 time series from ~10 different labeled regions in four mice. During the time-series acquisitions, the mice obtained rewards at a rate of 3.2 ± 0.7 rewards per min with a mean distance run between rewards of 2.5 ± 0.5 m, similar to reward rates during our previous electrophysiology experiments[15]. To extract the fluorescence versus time traces for the individual neurons, we first corrected the movies for brain motion that occurred during the acquisition using a two-dimensional cross correlation algorithm (see Online Methods). It was difficult to draw regions of interest (ROIs) manually around individual neurons because CA1 cell bodies are tightly packed together, GCaMP3 is found only in the cytoplasm (near the cell edges), and the axial extent of the imaging focal spot is probably more than ~4 μm (ref. 20). Instead, we used an automated cell identification method based on independent component analysis (ICA) and principal component analysis (PCA)[21,22]. Regions of interest for 10 neurons identified using this procedure are shown in red for the example field of view shown in **Figure 2a**. We extracted $\Delta F/F$ traces (**Fig. 2b**) from the ICA/PCA-defined ROIs. The $\Delta F/F$ traces revealed a baseline that was periodically interrupted by calcium transients that varied in amplitude (mean peak $\Delta F/F$ = 28 ± 32%), consistent with a difference in the number of underlying action potentials[13,23,24], and varied in duration (mean transient duration = 1.2 ± 1.1 s), consistent with the summation of multiple transients[12,13,25]. We identified significant transients with <5% false positive error rates[11,12] and used them in all subsequent analyses (see Online Methods; **Fig. 2b**,**c**). We used these traces as a surrogate measure of spiking activity and refer to them as the temporal activity patterns of the neurons.

In the 47 time-series datasets, we analyzed epochs in which the mouse performed goal-directed behavior to receive a reward (high reward rate epochs, see Online Methods). In nearly all of these datasets many individual neurons had location-specific activity. **Figure 2b** shows the temporal activity patterns of four neurons from the example field of view shown in **Figure 2a**, along with mouse position. When the mouse ran in the positive direction (left to right as seen in **Fig. 1c**), each of these four cells was active at a different location. This can be seen in the individual traversal (**Fig. 2c**) and in the plot of mean activity versus linear track position averaged over all 21 positive direction traversals (**Fig. 2d**,**e**). These plots reveal well-defined

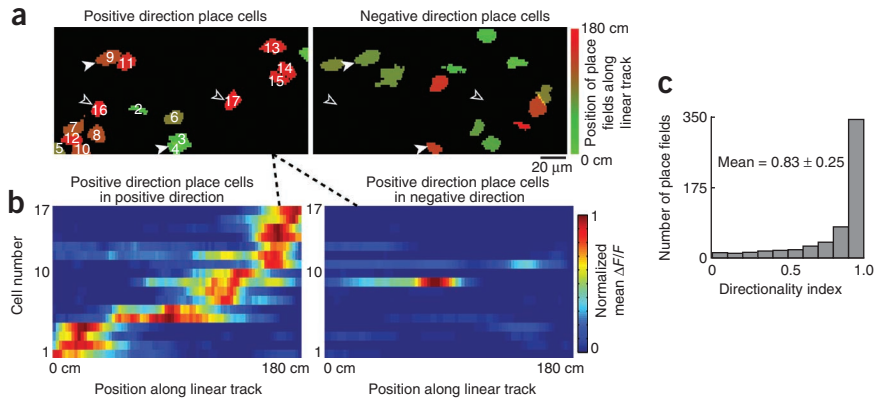


**Figure 3** Place cells differ depending on the running direction in the linear track. (**a**) An example imaging field in which the place cells are colored according to the location of their place fields along the virtual linear track. Significant place fields during running in the positive (left panel) and negative (right panel) directions are shown. Example place cells with different place fields or no place fields depending on the running direction are highlighted with closed arrowheads or open arrowheads, respectively. (**b**) A plot of mean $\Delta F/F$ versus linear track position for the positive direction place cells labeled in **a** (left) during running in the positive (left) and negative (right) directions. (**c**) Histogram of directionality index for all place fields.

and statistically significant fields of neuronal activity ($P < 0.05$ from bootstrapping, see Online Methods). The spatially restricted activity of these neurons and the well-defined shape of the activity fields were similar to extracellular recording measurements of place cells in real and virtual reality linear tracks[15,26,27]. Therefore, we concluded that these neurons are place cells. As well as identifying the place field for each of the place cells, imaging also reveals their exact relative anatomical locations (**Fig. 2f** and **Supplementary Movie 2**).

Consistent with previous studies[15,26], optically identified place cells had different place fields in the same environment depending on the direction of running (**Figs. 2b** and **3**). To analyze the directionality of activity during place field traversals, we divided the fluorescence time series into epochs defined by running direction. The mean fluorescence versus track position was calculated separately for each direction. A cell that had a place field during at least one direction of running was called a place cell; each place cell could therefore have up to two place fields. Many place cells had different place fields depending on the running direction (**Fig. 3a**) or had a place field for only one running direction (**Fig. 3a**). This high degree of directionality (**Fig. 3b**) was consistent across all datasets and was quantified for all place fields using a directionality index (0.83 ± 0.25, **Fig. 3c**; 1 represents high directionality, 0 represents no directionality; see Online Methods for definition).

Although we analyzed only high reward rate periods in the Results, we also analyzed place fields during different behavioral contexts[28–30] including the low reward rate periods (see **Supplementary Fig. 1**).

We found the main results of this research to be similar using either method of analysis (**Supplementary Fig. 2**).

Across our 47 time-series datasets, we identified 808 place cells and 881 place fields in those place cells. The mean total number of place cells per imaging field was 17 ± 9 and the mean total number of place fields per imaging field was 19 ± 10 (number of place cells with one place field was 735, number with two place fields was 73; 18 ± 6 complete runs through each place field). The calcium transients that defined these place fields had a mean duration of 1.1 ± 0.9 s (**Fig. 4a**) and a mean peak $\Delta F/F$ of 35 ± 29% (**Fig. 4b**). The distribution of place fields as a function of position along the track was inhomogeneous (**Fig. 4c**), as seen previously[31], with more centered between the reward sites and the towers (tall distal cues located ~60 cm from each end of the track; see **Fig. 1c**) than in the middle of the track. The mean width of the optically identified place fields was 50 ± 19 cm (**Fig. 4d**), which is ~20% larger than the mean width of place fields defined by firing rate in extracellular recordings under similar conditions[15] (41 ± 14 cm). To investigate this broadening, we convolved spike train electrophysiology recordings with model calcium transient waveforms (see Online Methods) and observed a similar increase in the resultant place field width (~20%; see **Supplementary Fig. 3**). This result is consistent with the idea that our place fields are defined by underlying spiking activity that is convolved with the time-broadening effects of intracellular calcium dynamics (**Supplementary Fig. 3**).

When optically identified place cells were active, the activity most frequently occurred in the place field; however, the place cells are not necessarily active during every traversal of the place field. This is similar to previous tetrode study reports of 'excess activity variance'[28] in place cells. **Figure 5a** shows the activity trace (temporal activity pattern) for each individual traversal of the mouse in the positive running direction for a subset of the place cells shown in **Figure 2**. Although place cells 2, 3, 6 and 9 are reliably active at the same location during nearly every traversal (active during >75% of traversals through the place field and active for >66% of the time spent in the place field), place cell 10 shows more variable activity. This cell is reliably active at the same location, but not during each traversal (active during 38% of traversals through the place field and active for 35% of the time spent in the place field). For all of the 881 place fields, the place cells were active during 65 ± 18% of traversals through the place field (**Fig. 5**) and active for 53 ± 17% of the time spent traversing through the place field (**Fig. 5**).

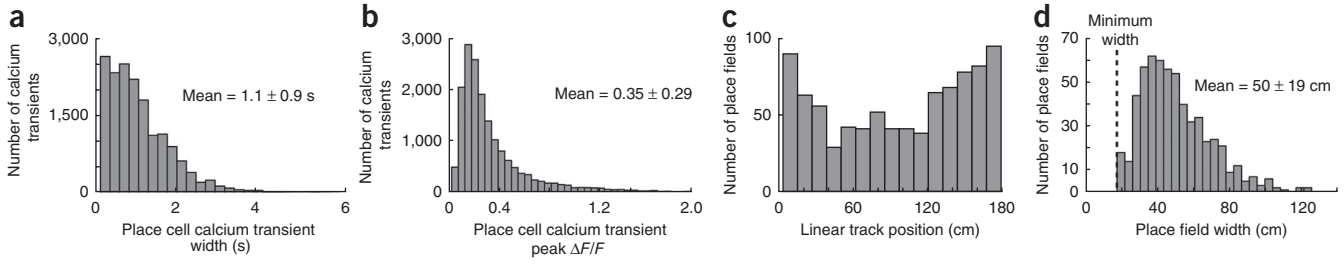


**Figure 4** Characterization of place cell calcium transients and place fields. Histograms of place cell transient widths (**a**) and transient peak $\Delta F/F$ (**b**) are shown for periods of mouse movement along the virtual track. Histograms of place field position along the linear track (**c**) and place field widths (**d**) are also shown.

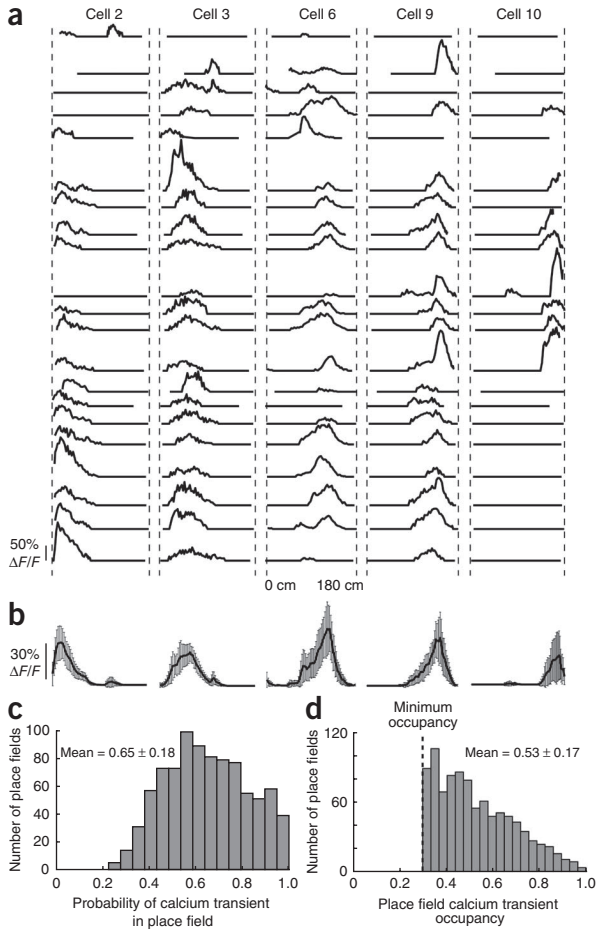


**Figure 5** Place cell activity variability in place fields. (**a**) Temporal activity pattern versus virtual linear track position traces for a subset of the cells shown in **Figure 2a** (right). Each of the 21 positive running direction track traversals is shown for each of the cells. (**b**) Mean and s.d. of $\Delta F/F$ versus linear track position for the traces shown in **a**. (**c**) Histogram of the probability that a place cell is active during traversals through the place field. (**d**) Histogram of the percentage of place field traversal time for which the cell had a significant calcium transient.

### Comparison with electrophysiology

We compared the properties of place cells measured optically in mice with hippocampal windows (cortical excavation and region infected with AAV2/1-*synapsin-1*-GCaMP3) with the same properties measured previously by electrophysiology in control mice (no cortical excavation or virus infection)[15]. The place field width in the mice with hippocampal windows (50 ± 19 cm) was very similar to that of the control mice (41 ± 14 cm)[15], and the effects of intracellular calcium dynamics in the presence of GCaMP3 can explain the ~20% broadening of the fields (**Supplementary Fig. 3**). The percentage of neurons that were place cells (~15–20%) in mice with hippocampal windows was similar to, but slightly less than, the percentage in our whole-cell patch clamp recording[15] (~20–30%). We also directly compared electrophysiologically measured place cell properties and local field potentials (LFPs) in mice with hippocampal windows (cortical excavation and region infected with AAV2/1-*synapsin-1*-GCaMP3) with the same measurements in control mice (no cortical excavation or virus infection)[15]. The LFP-recorded theta frequency in mice with hippocampal windows (7.3 ± 0.3 Hz, $n = 4$ mice; **Supplementary Fig. 4**) was very similar ($P = 0.32$, two-tailed $t$-test) to that of control mice (7.4 ± 0.2 Hz, $n = 11$ mice). The phase precession of spike times relative to LFP-recorded theta activity observed in control mice ($\Delta$phase = −73 ± 48°, $P < 0.01$; correlation between phase and position of spikes: correlation coefficient = −0.2 ± 0.1, $P < 0.01$; $n = 10$ place fields, 3 mice[15]) was similar in mice with hippocampal windows ($\Delta$phase = −104 ± 87°, $P < 0.01$; correlation between phase and position of spikes: correlation coefficient = −0.4 ± 0.3, $P < 0.01$; $n = 3$ place fields, 2 mice; **Supplementary Fig. 4**). Finally, theta-modulated high-frequency (>50 Hz) bursts of action potentials with decreasing spike amplitude that were characteristic of place cells in control mice were also found in mice with hippocampal windows (see inter-spike intervals in **Supplementary Fig. 4**).

These measurements show the similarity between place cells and CA1 network dynamics in mice with hippocampal windows compared with control rodents in both real and virtual environments[15,26,27]. Because our mice with hippocampal windows required cortical excavation and infection with AAV2/1-*synapsin-1*-GCaMP3, these results also show that viral infection, GCaMP3 expression, and cortical excavation did not substantially alter the hippocampal CA1 dynamics.

### The anatomical organization of CA1 place cells

We next examined the anatomical layout of place cells on the micrometer scale (see **Fig. 6a** for example fields of view). To quantify the

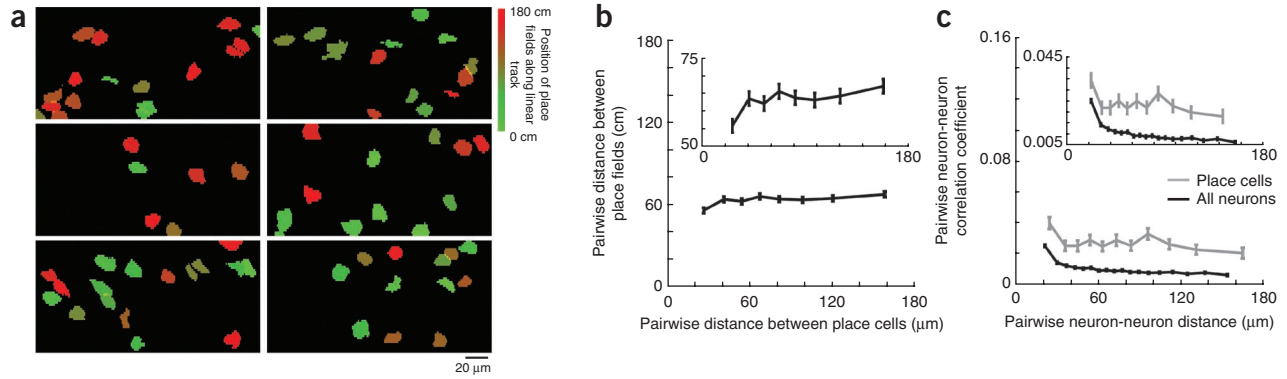


**Figure 6** Spatial organization of place cells in dorsal CA1. (**a**) Example images from different fields of view in which the place cells are colored according to the location of their place fields along the virtual linear track. Each image shows place cells with significant place fields during running in either the positive or negative direction. (**b**) Plot of mean distance between place cells in the hippocampus versus the mean distance between their place fields along the track averaged over all 47 time series. The error bars represent s.e.m. (**c**) Plot of mean distance between cells in the hippocampus versus the mean correlation between their temporal activity patterns averaged over all 47 time series for all place cells (gray) and all neurons (black). The error bars represent s.e.m.

relationship between anatomical location and place field location, we calculated all pairwise distances between place cells (distance between each cell's ROI center of mass) and pairwise distances between the peaks in their place fields separately for each running direction for each imaging field. We combined the results from all 47 datasets and plotted the mean distance between place fields as a function of mean distance between the place cells (**Fig. 6b**). For cells spaced over a wide range of distances, but excluding near-neighbors less than about 35 µm apart, we found a statistically insignificant relationship between the mean distance between place fields and the mean distance between the place cells (Spearman's rank correlation coefficient of 0.57, $P = 0.2$). Therefore, on average, the distance between place cells in the physical space of the hippocampus was not related to the distance between their place fields along the track when the place cells were more than about 35 µm apart (although there were some exceptions to this average rule; **Supplementary Fig. 1**). The data point that corresponded to the most closely neighboring place cells (less than about 35 µm apart) was significantly lower ($P < 0.025$, two-tailed $t$-test) than the points for all other distances between cells. This could be interpreted as fine-scale spatial clustering of place cells with similar place fields, but residual crosstalk, residual brain motion or a common neuropil signal between neighboring ROIs could also explain this result (see Discussion).

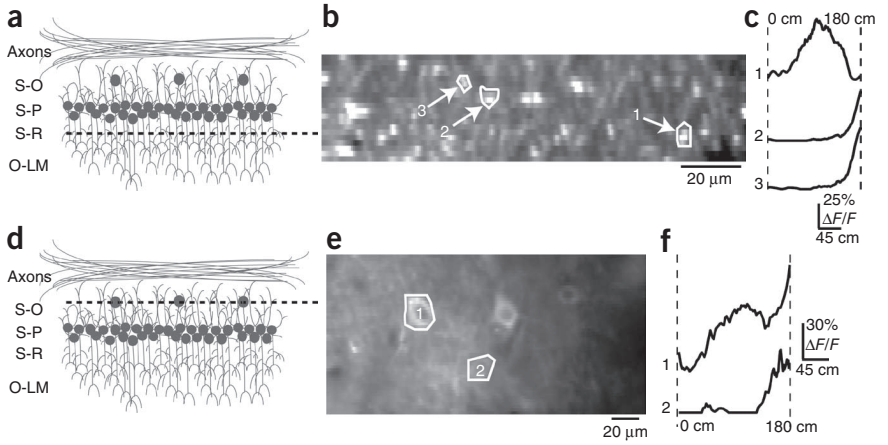


**Figure 7** Imaging place-related activity in dendrites and putative interneurons. (**a**,**b**) A two-photon image (**b**) of a field of view ~75 µm ventral to the stratum pyramidale cell body layer (dashed line in **a**). Bright spots in **b** are a cross-section through the apical dendrites from the overlying CA1 neurons. O-LM, oriens lacunosum molecular; S-O, stratum oriens; S-P, stratum pyramidale; S-R, stratum radiatum. (**c**) Mean $\Delta F/F$ versus linear track position for the dendrites labeled in **b**. (**d**,**e**) A two-photon image (**e**) of a field of view ~50 µm dorsal to the stratum pyramidale cell body layer (dashed line in **d**). Sparsely distributed cell bodies in **e** are assumed interneurons. (**f**) Mean $\Delta F/F$ versus linear track position for the interneurons labeled in the image in **e**.

We next studied whether the correlation between the temporal activity patterns of pairs of neurons varied as a function of the distance between them in the hippocampus. For all place cells in each imaging field, we calculated all pairwise temporal activity pattern correlations and pairwise distances between place cells and then combined the results from all 47 datasets. When we plotted the mean temporal correlation as a function of mean distance between the place cells (**Fig. 6c**), we found a statistically insignificant relationship (Spearman's rank correlation coefficient of −0.25, $P = 0.5$) for cells spaced more than about 35 µm apart. Again, the data point that corresponded to the near-neighbor place cells was statistically different ($P < 0.035$, two-tailed $t$-test) from all but one of the other data points. When we repeated this calculation for all neurons, including both place cells and non-place cells, the overall correlation was lower than for the place cells alone and there was a statistically significant relationship between mean temporal correlation and distance between the neurons (Spearman's rank correlation coefficient of −0.95, $P < 10^{-5}$; **Fig. 6c**), regardless of whether the data point for the most closely neighboring neurons was included.

### Imaging activity in dendrites and putative interneurons

To test whether our imaging method had the required resolution and signal-to-noise ratio to record activity patterns from dendrites, we acquired time series ~75 µm ventral to the stratum pyramidale (**Fig. 7**). In this plane, we could identify apical dendrites from the overlying pyramidal neurons (individual bright spots in **Fig. 7b**). When we plotted the mean activity versus linear track position, we found well-defined place fields in many of the apical dendrites (**Fig. 7c**). We imaged dendrites in four fields of view (~50 dendrites per field) in three mice and saw spatially modulated dendritic activity patterns in all of the fields. Back-propagating action potentials invade the dendritic arbors of CA1 pyramidal neurons[32,33]. Therefore, it is likely that the activity in the apical dendrites is due to opening of voltage-gated calcium channels induced by back-propagating action potentials rather than to the smaller calcium transients that are associated with synaptic input.

To show that our methods can be used to record from interneurons, we adjusted the imaging plane to ~50 µm dorsal to the stratum pyramidale (**Fig. 7d**) where we found sparsely distributed cell bodies (**Fig. 7e**). The neurons in this region of the stratum oriens have been identified as interneurons, suggesting that these cells are probably basket, oriens lacunosum moleculare or axo-axonic interneurons[34]. As in the stratum pyramidale, we found neurons with spatially modulated activity patterns in the stratum oriens (**Fig. 7f**); some of these had 'off' fields (**Fig. 7f**), as has been observed with extracellular recording[35,36]. We imaged interneurons in four fields of view (~2–3 interneurons per field) in two mice and found spatially modulated interneuron activity patterns in all of the fields.

## DISCUSSION

Our method relies on several combined technologies. We developed surgical methods to implant a hippocampal window that allowed chronic subcellular resolution imaging in the CA1 region of the hippocampus in behaving mice. The combination of this window with a custom two-photon microscope and background light suppression methods allowed imaging in mice that were interacting with a visual virtual reality system. Using the genetically encoded calcium indicator GCaMP3, our methods allowed us to study the spatially modulated activity patterns of pyramidal neurons in the stratum pyramidale, putative interneurons in the stratum oriens and apical dendrites in the stratum radiatum. By imaging the activity of populations of ~80–100 neurons in the stratum pyramidale in mice that had been trained to navigate along a virtual linear track, we identified place cells that had characteristics very similar to those of spiking rate-defined place cells in both real and virtual environments[15,26,27,37].

Tetrodes are the most common method used to record the activity of CA1 place cells in behaving mice. Tetrode array recordings

combined with spike-sorting procedures can be used to identify around five single units per tetrode[38,39]. Although sub-millisecond temporal resolution is a major advantage of this method compared to imaging, tetrode methods are limited by low spatial resolution (>100s of micrometers) and sparse sampling within the microcircuitry[38,40].

Our imaging method has several advantages over tetrode methods. For example, it is possible to report the precise anatomical position of functionally identified neurons within the microcircuitry. Imaging also allows researchers to make functional recording from subcellular compartments, to identify all neurons (even silent cells), and to take advantage of the growing number of available genetic tools[41]. It should be possible to image subcellular dynamics such as signal transduction[42] and structural plasticity[43] in the context of learning and memory during behavioral paradigms. In addition, optical methods might allow researchers to identify the functional properties of specific neurons in a large population, followed by either the subsequent reconstruction of the underlying connections[44] or modification of their activity[45]. Finally, imaging methods can allow the unambiguous identification and recording of the same neurons over many weeks. Although this was not the focus of this research, to address the technical feasibility of such studies we have imaged the same region of CA1 over multiple days (**Supplementary Fig. 5**).

Here we assumed that calcium transients could be used as a proxy for spiking activity. Sodium action potentials generate calcium transients in GCaMP3-expressing hippocampal pyramidal neurons in brain slices. Calcium transient amplitude increases linearly with the number of evoked action potentials, until saturation at more than about 10 action potentials[13]. There is a quantitatively similar relationship between spiking activity and calcium transient amplitude for neocortical neurons in brain slices and *in vivo* in both anesthetized and awake mice[13]. It is therefore reasonable to assume that the spiking activity of the CA1 neurons *in vivo* generated calcium transients similar to those seen in slices[13]. Using these previous calcium transient measurements[13] and our extracellular place cell recordings, we calculated the spike-induced calcium transients that would be expected in our imaging experiments (**Supplementary Fig. 3**). The characteristics of the optically defined place fields are consistent with and can be fully explained by calcium transients induced by sodium action potentials. Therefore, the contribution of other sources to our calcium transients, such as calcium influx due to synaptic input or dendritic calcium spikes, is probably small.

It is unlikely that our methods allow us to detect single action potentials[13], to determine firing rates or to reliably count the number of spikes. Although these limitations probably do not pose a problem for identifying place fields in place cells owing to the marked increase in spiking rate in the place field and the ability to average over many traversals, it is still possible that place cells with low activity levels may not be detected.

Cortical excavation was used to expose the hippocampus for acute electrophysiology experiments in anesthetized cats nearly 50 years ago[46]. More recently, cortical excavation was combined with the use of a polystyrene tube filled with agarose and sealed with a coverslip to facilitate two-photon imaging of dendritic spines in an acute, anesthetized mouse preparation[14]. Here, we used these methods as a starting point to develop a chronic hippocampal window designed for imaging in behaving mice. The stainless steel cannula and coverslip directly bonded to the external capsule surface with Kwik-Sil formed a rigid support structure that minimized brain motion during animal movements and allowed repeated imaging of the hippocampus for weeks. The removal of the cortex overlying the hippocampus did not detectably alter the mouse's performance of the task, or the hippocampal dynamics and place cell properties that were measured in our preparation compared to those of control mice.

Miniaturized head-mounted microscopes[47,48] may allow hippocampal imaging in freely moving animals. Such experiments would benefit from the natural array of inputs, as opposed to the lack of vestibular input and potentially altered gait of our mice. Our methods, however, have the advantages of not requiring a miniaturized microscope, easy combination with electrophysiology, and the potential to manipulate specific environmental cues using virtual reality in ways that would be difficult or impossible in real environments.

We used an ICA/PCA algorithm to identify individual neurons on the basis of both their spatial and temporal characteristics[21]. However, this method could not identify silent neurons and occasionally missed active cells, making it hard to estimate the number of potentially active neurons. Therefore, it was difficult to quantify the exact fraction of neurons that were place cells. Based simply on the morphology of neurons in the fields of view, we estimate that our fields contained ~80–100 neurons, meaning that ~15–20% of the neurons were place cells, slightly less than previous estimates[15]. In addition to the uncertain number of potentially active neurons, this slight difference could also be due to differences in the recording methods and differences in the definitions of place fields.

The ICA/PCA algorithm was successful in limiting the crosstalk between neighboring ROIs. However, when studying the spatiotemporal organization of neurons in CA1, we could not rule out the possibility of residual crosstalk, residual brain motion or a common neuropil signal between the most closely neighboring cells (less than about 35 μm). This is one possible explanation for the statistically outlying data points in **Figure 6b**,**c** that correspond to the most closely neighboring cells. An alternative explanation for these outlying data points is that they represent small clusters of functionally similar neurons, as recent studies have suggested[5,9].

For place cells that were further separated (more than about 35 μm), the distance between their place fields along the track was statistically unrelated to the distance between their positions in the hippocampus. A few previous electrode recording studies found anatomically organized clusters of functionally similar hippocampal neurons on the 0.6–1 mm spatial scale[6,7], whereas a separate study of CA1 place cell location concluded that there was a lack of anatomical spatial organization[8]. These previous methods provided only an indirect measure of the spatial organization of place cells in the CA1 microcircuitry. By contrast, using our methods, we were able to directly measure the spatial organization. Although possible crosstalk concerns meant that we could not unambiguously measure the organization down to the finest scale, it was possible to conclude that place cells are anatomically distributed down to a scale of at least ~35 μm.

For place cells separated by at least this scale, there was also no relationship between the correlation between their temporal activity patterns and the physical distance between them. For all neurons, we found a statistically significant decrease in temporal correlation between the neurons the further they were from each other in the physical space of the hippocampus (**Fig. 6**). Although this decrease is significant, both the overall correlation and the rate at which the correlation decreases as a function of distance are nearly an order of magnitude smaller than has been observed in the motor cortex of behaving mice[11].

Finally, we note that spatiotemporal organization can occur in many forms, most of which were not examined here. The methods outlined in this research should allow future studies to search more thoroughly for micro-organization within the hippocampus.

## METHODS

Methods and any associated references are available in the online version of the paper at http://www.nature.com/natureneuroscience/.

*Note: Supplementary information is available on the Nature Neuroscience website.*


### ACKNOWLEDGMENTS

This work was supported by Princeton University, the National Institutes of Health (grant 5R01MH083686-03), The Howard Hughes Medical Institute, The Helen Hay Whitney Foundation and The Patterson Trust. We thank F. Collman for the brain motion correction algorithm.


### AUTHOR CONTRIBUTIONS

D.A.D. and D.W.T. designed the research. D.A.D. performed the imaging experiments and developed the chronic hippocampal window system and surgery/training sequences. D.W.T. designed and implemented the combined two-photon microscope and virtual reality instrumentation. D.A.D. and C.D.H. performed extracellular recording and optimized virtual reality training procedures. L.T. and L.L.L. provided AAV2/1-*synapsin-1*-GCaMP3. D.A.D. analyzed the data. D.A.D. and D.W.T. wrote the paper.

### COMPETING FINANCIAL INTERESTS

The authors declare no competing financial interests.

Published online at http://www.nature.com/natureneuroscience/.
Reprints and permissions information is available online at http://www.nature.com/reprintsandpermissions/.




1. O'Keefe, J. & Dostrovsky, J. The hippocampus as a spatial map. Preliminary evidence from unit activity in the freely-moving rat. *Brain Res.* **34**, 171–175 (1971).
2. Ergorul, C. & Eichenbaum, H. The hippocampus and memory for "what," "where," and "when." *Learn. Mem.* **11**, 397–405 (2004).
3. O'Keefe, J. Hippocampal neurophysiology in the behaving animal. in *The Hippocampus Book* (ed. P. Andersen) 475–548 (Oxford University Press, Oxford, 2007).
4. Leutgeb, S., Leutgeb, J.K., Moser, M.B. & Moser, E.I. Place cells, spatial maps and the population code for memory. *Curr. Opin. Neurobiol.* **15**, 738–746 (2005).
5. Nakamura, N.H. *et al.* Hippocampal cells encode places by forming small anatomical clusters. *Neuroscience* **166**, 994–1007 (2010).
6. Eichenbaum, H., Wiener, S.I., Shapiro, M.L. & Cohen, N.J. The organization of spatial coding in the hippocampus: a study of neural ensemble activity. *J. Neurosci.* **9**, 2764–2775 (1989).
7. Hampson, R.E., Simeral, J.D. & Deadwyler, S.A. Distribution of spatial and nonspatial information in dorsal hippocampus. *Nature* **402**, 610–614 (1999).
8. Redish, A.D. *et al.* Independence of firing correlates of anatomically proximate hippocampal pyramidal cells. *J. Neurosci.* **21**, RC134 (2001).
9. Takahashi, S. & Sakurai, Y. Sub-millisecond firing synchrony of closely neighboring pyramidal neurons in hippocampal CA1 of rats during delayed non-matching to sample task. *Front. Neural Circuits* **3**, 9 (2009).
10. Denk, W., Strickler, J.H. & Webb, W.W. Two-photon laser-scanning fluorescence microscopy. *Science* **248**, 73–76 (1990).
11. Dombeck, D.A., Graziano, M.S. & Tank, D.W. Functional clustering of neurons in motor cortex determined by cellular resolution imaging in awake behaving mice. *J. Neurosci.* **29**, 13751–13760 (2009).
12. Dombeck, D.A., Khabbaz, A.N., Collman, F., Adelman, T.L. & Tank, D.W. Imaging large-scale neural activity with cellular resolution in awake, mobile mice. *Neuron* **56**, 43–57 (2007).
13. Tian, L. *et al.* Imaging neural activity in worms, flies and mice with improved GCaMP calcium indicators. *Nat. Methods* **6**, 875–881 (2009).
14. Mizrahi, A., Crowley, J.C., Shtoyerman, E. & Katz, L.C. High-resolution *in vivo* imaging of hippocampal dendrites and spines. *J. Neurosci.* **24**, 3147–3151 (2004).
15. Harvey, C.D., Collman, F., Dombeck, D.A. & Tank, D.W. Intracellular dynamics of hippocampal place cells during virtual navigation. *Nature* **461**, 941–946 (2009).
16. Hölscher, C., Schnee, A., Dahmen, H., Setia, L. & Mallot, H.A. Rats are able to navigate in virtual environments. *J. Exp. Biol.* **208**, 561–569 (2005).
17. Denk, W. & Svoboda, K. Photon upmanship: why multiphoton imaging is more than a gimmick. *Neuron* **18**, 351–357 (1997).
18. Thiel, G., Greengard, P. & Sudhof, T.C. Characterization of tissue-specific transcription by the human synapsin I gene promoter. *Proc. Natl. Acad. Sci. USA* **88**, 3431–3435 (1991).
19. Burger, C. *et al.* Recombinant AAV viral vectors pseudotyped with viral capsids from serotypes 1, 2, and 5 display differential efficiency and cell tropism after delivery to different regions of the central nervous system. *Mol. Ther.* **10**, 302–317 (2004).
20. Ji, N., Milkie, D.E. & Betzig, E. Adaptive optics via pupil segmentation for high-resolution imaging in biological tissues. *Nat. Methods* **7**, 141–147 (2010).
21. Mukamel, E.A., Nimmerjahn, A. & Schnitzer, M.J. Automated analysis of cellular signals from large-scale calcium imaging data. *Neuron* **63**, 747–760 (2009).
22. Reidl, J., Starke, J., Omer, D.B., Grinvald, A. & Spors, H. Independent component analysis of high-resolution imaging data identifies distinct functional domains. *Neuroimage* **34**, 94–108 (2007).
23. Kerr, J.N., Greenberg, D. & Helmchen, F. Imaging input and output of neocortical networks *in vivo*. *Proc. Natl. Acad. Sci. USA* **102**, 14063–14068 (2005).
24. Sato, T.R., Gray, N.W., Mainen, Z.F. & Svoboda, K. The functional microarchitecture of the mouse barrel cortex. *PLoS Biol.* **5**, e189 (2007).
25. Greenberg, D.S., Houweling, A.R. & Kerr, J.N. Population imaging of ongoing neuronal activity in the visual cortex of awake rats. *Nat. Neurosci.* **11**, 749–751 (2008).
26. McNaughton, B.L., Barnes, C.A. & O'Keefe, J. The contributions of position, direction, and velocity to single unit activity in the hippocampus of freely-moving rats. *Exp. Brain Res.* **52**, 41–49 (1983).
27. Nakazawa, K. *et al.* Hippocampal CA3 NMDA receptors are crucial for memory acquisition of one-time experience. *Neuron* **38**, 305–315 (2003).
28. Fenton, A.A. & Muller, R.U. Place cell discharge is extremely variable during individual passes of the rat through the firing field. *Proc. Natl. Acad. Sci. USA* **95**, 3182–3187 (1998).
29. Frank, L.M., Brown, E.N. & Wilson, M. Trajectory encoding in the hippocampus and entorhinal cortex. *Neuron* **27**, 169–178 (2000).
30. Griffin, A.L., Eichenbaum, H. & Hasselmo, M.E. Spatial representations of hippocampal CA1 neurons are modulated by behavioral context in a hippocampus-dependent memory task. *J. Neurosci.* **27**, 2416–2423 (2007).
31. Gupta, A.S., van der Meer, M.A., Touretzky, D.S. & Redish, A.D. Hippocampal replay is not a simple function of experience. *Neuron* **65**, 695–705 (2010).
32. Regehr, W.G., Connor, J.A. & Tank, D.W. Optical imaging of calcium accumulation in hippocampal pyramidal cells during synaptic activation. *Nature* **341**, 533–536 (1989).
33. Spruston, N., Schiller, Y., Stuart, G. & Sakmann, B. Activity-dependent action potential invasion and calcium influx into hippocampal CA1 dendrites. *Science* **268**, 297–300 (1995).
34. Klausberger, T. *et al.* Brain state– and cell type–specific firing of hippocampal interneurons *in vivo*. *Nature* **421**, 844–848 (2003).
35. Ego-Stengel, V. & Wilson, M.A. Spatial selectivity and theta phase precession in CA1 interneurons. *Hippocampus* **17**, 161–174 (2007).
36. Wilent, W.B. & Nitz, D.A. Discrete place fields of hippocampal formation interneurons. *J. Neurophysiol.* **97**, 4152–4161 (2007).
37. Schnee, A. *Rats in Virtual Reality: The Development of an Advanced Method to Study Animal Behaviour* (Eberhard-Karls-University, Tübingen, 2008).
38. Buzsáki, G. Large-scale recording of neuronal ensembles. *Nat. Neurosci.* **7**, 446–451 (2004).
39. Wilson, M.A. & McNaughton, B.L. Dynamics of the hippocampal ensemble code for space. *Science* **261**, 1055–1058 (1993).
40. Henze, D.A. *et al.* Intracellular features predicted by extracellular recordings in the hippocampus *in vivo*. *J. Neurophysiol.* **84**, 390–400 (2000).
41. Luo, L., Callaway, E.M. & Svoboda, K. Genetic dissection of neural circuits. *Neuron* **57**, 634–660 (2008).
42. Miyawaki, A. Visualization of the spatial and temporal dynamics of intracellular signaling. *Dev. Cell* **4**, 295–305 (2003).
43. Holtmaat, A. & Svoboda, K. Experience-dependent structural synaptic plasticity in the mammalian brain. *Nat. Rev. Neurosci.* **10**, 647–658 (2009).
44. Denk, W. & Horstmann, H. Serial block-face scanning electron microscopy to reconstruct three-dimensional tissue nanostructure. *PLoS Biol.* **2**, e329 (2004).
45. Boyden, E.S., Zhang, F., Bamberg, E., Nagel, G. & Deisseroth, K. Millisecond-timescale, genetically targeted optical control of neural activity. *Nat. Neurosci.* **8**, 1263–1268 (2005).
46. Kandel, E.R., Spencer, W.A. & Brinley, F.J. Jr. Electrophysiology of hippocampal neurons. I. Sequential invasion and synaptic organization. *J. Neurophysiol.* **24**, 225–242 (1961).
47. Helmchen, F., Fee, M.S., Tank, D.W. & Denk, W. A miniature head-mounted two-photon microscope. high-resolution brain imaging in freely moving animals. *Neuron* **31**, 903–912 (2001).
48. Sawinski, J. *et al.* Visually evoked activity in cortical cells imaged in freely moving animals. *Proc. Natl. Acad. Sci. USA* **106**, 19557–19562 (2009).

## ONLINE METHODS

**Two-photon microscope and data acquisition.** Our microscope design is shown in **Figure 1a**. Focusing control was achieved by mounting the microscope objective on a single-axis piezo-motorized translation stage (Z-translation; Agilis AG-LS25) within the microscope. X-Y control was achieved by mounting the spherical treadmill and mouse head-restraint on a manual actuator-driven translation stage.

The microscope was built out of custom-machined and black anodized aluminum parts and was designed to entirely enclose all of the internal optics except for one hole for the microscope objective and one hole for the entry of the excitation laser beam. The first step in mitigating stray light entry into the microscope was to create precise fitting lips at every joint between any two pieces of the outer shell of the microscope. This had the effect of eliminating nearly all light entry through the outer body of the enclosed microscope. The first major point of entry for stray light into the microscope was then the excitation laser input port. A long-pass colored glass filter (Thorlabs, 780 long pass) covered this hole to allow only the excitation laser light to pass, but not the shorter wavelength light from the projection system. The second point of entry for stray light was the hole for the microscope objective (Olympus 40×, 0.8 NA). To combat light entry at this point, one end of a loose tube of thin black rubber was attached to the microscope around the objective (**Fig. 1d**). The other end of the tube was attached to a metal ring that was machined to tightly fit around a separate ring that was cemented to the top of the headplate and centered around the craniotomy. The flexibility of the thin rubber allowed movement of the microscope objective with respect to the craniotomy while maintaining the light-tight connections at both ends of the rubber tube. It was also possible for stray light (especially longer wavelength red light) to enter the microscope by traveling through the animal and subsequently through the exposed skull between the craniotomy and the inner edge of the metal ring that was attached to the animal's skull. This area was therefore covered with opaque dental cement (Meta-bond, Parkell, made opaque by adding India Ink at ~5% vol/vol) so that the only remaining source of stray light through the microscope objective hole was through the hippocampal window itself (**Fig. 1e**). The light through this window proved to be inconsequential in the green imaging channel (<~5% of the baseline fluorescence level from labeled cells). Though red fluorophores were not used in this research, we found that a red light blocking filter (for example, 500/40, Chroma) in front of the projector was needed to reduce the amount of stray light in the red imaging channel to <~5% of the baseline fluorescence level from labeled cells.

The Ti:sapphire excitation laser (Chameleon Ultra II, Coherent) was operated at 920 nm (~30–50 mW average power at the sample). Green GCaMP3 fluorescence was isolated using a bandpass filter (Semrock, 542/50) and detected using a GaAsP PMT (1077P-40, Hamamatsu). ScanImage (v3.6)[49] was used for microscope control and acquisition. Images (256 × 64 pixels, ~200 × 100 µm field of view) were acquired at 15.6 Hz. During the ~9–13 min of time-series acquisition at a single location, photo-bleaching was observed at a mean rate of ~1–2% per minute.

Our spherical treadmill and virtual reality system has been described[12,15]. We used a Digidata (Axon Instruments, 1440A) data acquisition system to record (Clampex 10.2) and synchronize position in the linear track, reward timing and two-photon image frame timing (using the command signal to the slow galvanometer). Instead of the MX-1000 computer mouse used previously, here we used an MX-518 (Logitech) mouse to record ball rotation. The ball movements measured using the LED based MX-518 mouse were less sensitive to the exact distance between the sensor and ball surface than the MX-1000. In addition, the MX-518 mouse can be adjusted between three gain settings, the lowest of which allowed measurements of larger ball velocity without saturation than the MX-1000.

**Mouse training, hippocampal window and AAV injections.** All experiments were performed in compliance with the Guide for the Care and Use of Laboratory Animals (http://www.nap.edu/readingroom/books/labrats/). Specific protocols were approved by the Princeton University Institutional Animal Care and Use Committee. Imaging experiments were performed on five male C57BL/6 mice (postnatal day ~50). First, mice were anesthetized (Isoflurane, ~1%), a headplate was attached to the skull using opaque metabond and the stereotactic coordinates overlying the hippocampus were marked (1.8 mm lateral, 2.0 mm caudal to bregma). Any exposed skull was covered with a silicone elastomer (Kwik-Sil, World Precision Instruments). Anesthesia was then removed and the mouse recovered. Beginning the next day, the mice were put on a water restriction regimen so that they received 1 ml of water per day. After ~5–7 days, final body weight was ~80% of the before restriction weight. Training then began in the virtual linear track (one ~45 min session per day) and continued until the mice routinely ran back and forth along the linear track to achieve a high reward rate (~2 rewards per minute); this required ~10 training sessions. The mice were trained the same and the learning was the same as previously[15].

The mice were then anesthetized and a small (~0.5–1.0 mm) craniotomy was made at the previously marked spot on the skull overlying the dorsal hippocampus. Three injections of a solution containing AAV2/1-*synapsin-1*-GCaMP3 were made (~30 nl per injection, ~5 min per injection) ~200 µm apart at a depth of ~1,300 µm below the dural surface using a beveled glass micropipette (~2 MΩ after beveling). The craniotomy and any exposed skull were again covered with Kwik-Sil. The mice then recovered from anesthesia. For 2 d prior to the injections, the mice received 3 ml of water per day.

After 24–48 h, the mice were re-anesthetized and a trephine drill (Fine Science Tools) was used to cut a ~2.7–2.8-mm diameter craniotomy centered over the previously made small craniotomy. The dura was then removed with forceps and aspiration was used to slowly remove the cortex within the craniotomy. The removal was accomplished very slowly with aspiration of ~50–100 µm of tissue at a time followed by repeated irrigation with saline until any bleeding stopped. These steps continued until the external capsule was exposed. The cortex and top-most layers of the external capsule were 'peeled away' so that the remaining external capsule was never physically touched. To reduce animal movement-induced brain motion that could interfere with time-series image acquisition, the surface of the external capsule was allowed to dry until tacky, a small drop of uncured Kwik-Sil was applied to the surface, and then the cannula was inserted (with a few hundred micrometers left above the skull surface) and cemented to the skull using opaque Meta-bond. When cured, the small drop of Kwik-Sil had the effect of bonding the cannula to the external capsule and reducing in-focal plane (X-Y) brain motion. In some cases, the cannula did not fit through the craniotomy and a hand drill was used to slightly widen the hole. After this hippocampal window implantation surgery, the mice typically woke up after ~10 min and were walking around the cage within ~15 min. The next day, training in the virtual linear track resumed as before the surgery. Approximately 7 days after the window surgery, imaging experiments began. The experiments took place every 2–3 days for up to ~3–4 weeks in the same mouse (up to ~4–5 weeks after the window surgery). GCaMP3 expression reached a somewhat steady state level ~14 days after injection. A small fraction of nuclear-filled GCaMP3 neurons with altered physiology have been described in the cortex[13]. A similar small fraction of nuclear-filled neurons were observed here in CA1 (starting ~2–3 weeks after injection). These neurons often generated large, long-duration calcium transients that rarely defined a place field.

The cannula was composed of a 1.5-mm segment of a 2.77 mm outer diameter and 2.31 mm inner diameter thin-walled stainless steel tube (Small Parts Inc.). A 2.5-mm diameter round coverglass (Erie Scientific, Thermo Scientific) was cemented to one end of the tubing using UV curable adhesive (Norland Products).

**Does cortical excavation alter hippocampal dynamics and place cell properties?** To image the CA1 region of the hippocampus with cellular resolution, it was necessary to unilaterally remove part of the overlying cortex (including parietal cortex and parts of visual and hindlimb sensory cortex). This raises the concern that cellular and network properties within the hippocampus may be altered either by direct mechanical trauma to the hippocampus or by altering upstream inputs to the hippocampus due to the cortical lesion (although the excavated cortical regions do not provide strong direct projections to the hippocampal region). Regarding mechanical trauma, our surgical procedures allow the removal of the overlying cortex without the need to physically touch the surface of the hippocampus. The cortex and the top-most axons in the external capsule were 'peeled away' from the remaining external capsule without applying direct pressure or inadvertent mechanical trauma to the hippocampus. Furthermore, the external capsule itself provides a protective barrier to the underlying CA1 region of the hippocampus. Therefore, overt signs of damage, such as vesiculated dendrites or reduced or aberrant neuronal activity observed via calcium transients, were not observed. Although overt signs of damage were easily avoided, more subtle effects due to alterations of the upstream circuits projecting to the hippocampus were still possible. However, the properties of CA1 place cells measured

electrophysiologically and optically in our hippocampal window mice (cortical excavation and region infected with AAV2/1-*synapsin-1*-GCaMP3) were found to be similar to the same properties measured previously with electrophysiology in control mice (no cortical excavation or virus infection; see Results). Additionally, no significant difference was observed in the task performance of the same mice in the 4 days before the hippocampal window surgery compared to the 7 days after the surgery ($1.7 \pm 1.2$ versus $1.8 \pm 0.6$ rewards per min, respectively, $P = 0.51$, two-tailed *t*-test, $n = 5$ mice, one ~45-min session per mouse per day).

**Bolus loading of calcium indicators in CA1.** We first attempted to use multi-cell bolus loading[50] of the exogenous indicator Oregon Green Bapta-1-AM. Although we could label large populations of CA1 neurons and record their activity, this method had the drawback of only labeling cells for a few hours. In addition, we could only label cells immediately before the cannula was implanted, meaning that the imaging experiments had to be performed on the same day as the cortical excavation procedure and during the short time window after the mice awoke from surgery but before the cell labeling disappeared. During these periods, the mice rarely performed well at the task. A few place cells per field could be identified during periods of running, but the percentage of cells that were place cells (<~5%) and the width of the place fields (~2–3 times greater than expected from our electrophysiology measurements[15]) indicated altered hippocampal place cell and/or network dynamics. Because of these limitations, and the advantages of genetically encoded indicators, we used GCaMP3 (ref. 13).

**Data analysis.** Analysis was performed using ImageJ (1.40 g) and custom scripts written in MatLab (version 7). All data in the text and figures are presented as mean ± s.d., except in the plots shown in **Figure 6b,c** and **Supplementary Figure 2**, where the error bars represent s.e.m.

Time-series datasets were motion corrected using whole-frame cross-correlation. Although our previously published HMM line-by-line motion correction algorithm[12] would probably provide superior correction, our imaging frame rate (~15 Hz) was fast enough that in-frame distortions were minimal using whole-frame correction. In addition, it was more straightforward to apply the ICA/PCA cell ROI selection algorithm to the whole-frame corrected time-series than to the HMM-corrected time-series in which blank lines made automatic ROI detection difficult. The mean frame-to-frame in-plane (X-Y) Euclidean distance brain motion during all time periods (the mice ran almost continuously during our time-series acquisitions) was $1.8 \pm 1.3$ μm; the motion during periods of mouse movement along the virtual track used to define place fields (see below) was $1.5 \pm 1.2$ μm. Out of plane (Z) motion (measured as described[12]) was measured in untrained mice running on a spherical treadmill; during periods of running the Z-motion was $0.7 \pm 0.2$ μm.

ROIs were defined as described previously[21] (mu = 0.5, 150 principal components, 100 independent components, s.d. threshold = 1.25, 60 pixels < area of ROI < 400 pixels). Manual inspection revealed that the ROIs nearly always defined single cell regions. $\Delta F/F$ versus time traces were generated for each ROI. Slow time-scale changes in the fluorescence traces were removed by examining the distribution of fluorescence in a ~15-s interval around each sample time point and subtracting the 8% percentile value. The baseline-subtracted neuron fluorescence traces were then subjected to analysis of the ratio of positive- to negative-going transients of various amplitudes and durations as described[12]. We used this analysis to identify significant transients with <5% false positive error rates and generated the significant transient-only traces (**Figs. 2b,c** and **5a**) that were used for all subsequent analysis[11]. Note that the significant transient only traces are not discontinuous traces; the significant transients are left untouched, but the time points between the significant transients are all set to 0.

Place fields were identified and defined as follows. Long running periods of mouse movement along the virtual track in which the virtual velocity was >8.3 cm $s^{-1}$ and the run length was >53 cm (straight run without changing direction or hitting the end of the track) were identified. These periods were first categorized based on the direction of running (positive or negative direction). Positive and negative long running direction periods were then further subdivided into two categories based on the animal's current performance of the task. Segments of time between two rewards in which long running periods of only one direction occurred were defined as high reward rate periods, all other long running periods were defined as low reward rate periods. Timeseries datasets were only included if a mean of at least 10 long running segments during high reward rate periods in the positive and negative directions were completed during time series acquisition (this occurred in 47 datasets). Only high reward rate periods were analyzed, except in **Supplementary Figures 1**,**2** and **5** where the low reward rate periods were also included as a comparison (note that for the analysis in these figures the requirement of a mean of at least 10 long running/high reward periods was dropped, allowing the inclusion of additional datasets: 103 datasets total). For each running direction (during high reward rate periods) for each cell, the mean $\Delta F/F$ was calculated as a function of virtual position for 80 position bins and this mean fluorescence versus position plot was then smoothed (averaged) over three adjacent points. Potential place fields were first identified as contiguous regions of this plot in which all of the points were greater than 25% of the difference between the peak $\Delta F/F$ value (for all 80 bins) and the baseline value (mean of the lowest 20 out of 80 $\Delta F/F$ values). These potential place field regions then had to satisfy the following criteria. (i) The field must be >18 cm wide. (ii) The field must have one value of at least 10% mean $\Delta F/F$. (iii) The mean in-field $\Delta F/F$ value must be more than three times the mean out-of-field $\Delta F/F$ value. (iv) Significant calcium transients must be present >30% of the time the mouse spent in the place field. Potential place field regions that met these four criteria were then defined as place fields if their *P*-value from boot strapping was <0.05. Bootstrapping was performed by breaking the $\Delta F/F$ trace for each cell into at least nine segments (determined by the significant transients) that were randomly shuffled. The mean shuffled $\Delta F/F$ versus position plots were then subjected to the same criteria outlined above. This process was repeated 1,000 times and the *P*-value was defined as the ratio of the number of times out of 1,000 that the random shuffled trace generated a place field that met the above criteria.

A directionality index for mean $\Delta F/F$ in a place field in positive and negative running directions ($F_+$, $F_-$) was defined as $|F_+ - F_-|/(F_+ + F_-)$. A directionality index of 0 indicates identical activity in both directions, whereas an index of 1 indicates activity in one direction only.

Note that while very little movement along the width of the virtual linear track was possible, this position as well as the view angle were not controlled for in our analysis. These factors could contribute to increased variability of the place fields. Also note that during time-series acquisition, the mice rarely stopped in the middle (between reward zones) of the track (**Supplementary Fig. 1**): only $5 \pm 3\%$ of the time per time series was the virtual velocity <0.05 cm $s^{-1}$ in the middle of the track.

Correlation values were defined as the Pearson's correlation coefficient. Correlation versus distance between neuron and place field distance versus distance between neuron plots were generated from imaging fields that had at least two place cells and any two cells that had overlapping ROIs were excluded from the analysis. The position of a place field along the virtual track was defined as the position within the field with the maximal $\Delta F/F$ value. For the mean place field width calculation, only fields in which neither field edge was at the end of the track were included. This avoided the inclusion of fields that were artificially narrow due to clipping at one end of the track.

**Electrophysiology.** Extracellular place cell recordings were performed in four mice with hippocampal windows using methods similar to those described[15]. All procedures for these mice were identical to those used in imaging experiments (water restriction, training, virus injection, surgeries, and so on) except that a small hole (~0.5 mm) was drilled in the center of the window coverslip before implantation. After implantation, this small hole allowed electrode access to the hippocampus through the cannula. A tungsten metal electrode (3 MΩ impedance at 1 kHz, FHC) or glass microelectrode (resistance ~2.5 MΩ, filled with 0.5 M NaCl) recorded CA1 extracellular currents that were amplified (DAM80, WPI or AxoClamp 2B) and filtered (3 Hz–10 kHz, Brown-Lee Model 440) before being digitized at 20 kHz with a Digidata (Axon Instruments, 1440A). Note that this preparation was intended to mimic the conditions of the imaging experiments, but did not allow long-duration extracellular recordings; the hole in the coverslip to allow electrode access probably caused instability due to reduced stabilizing pressure. While these recordings (~3–5 min duration per cell) allowed clear identification of place cells and phase precession, the reduced number of passes through the place field compared to longer recordings led to noisier place field maps and phase precession plots (**Supplementary Fig. 4**). To reduce low frequency (<~50 Hz) electrical noise observed during treadmill rotation, the ball was coated with unscented fabric softener (Ultra Downy, Procter and Gamble) and allowed to dry overnight for electrical recordings. In other experiments not reported here, treating the ball with




doi:10.1038/nn.2648

Benz-all or anti-static sprays also reduced this noise. Further work will be required to determine whether this noise is a result of charge buildup on the ball.

Spikes were sorted offline using a threshold analysis. At most one unit was isolated from a single recording. Spike waveforms were overlayed and inspected visually to make sure that they matched (**Supplementary Fig. 4**), and inter-spike interval distributions were plotted to make sure no spikes fell within the refractory period (1–2 ms; **Supplementary Fig. 4**). To create firing rate maps (**Supplementary Figs. 3** and **4**), we divided the virtual linear track into 80 bins and calculated the firing rate as the total number of spikes in a bin divided by the total amount of time spent in a bin. To identify place fields, we found groups of adjacent bins with firing rates greater than 0.25 times the rate in the peak bin. We selected only those fields that were larger than 8 bins (18 cm) in length, had mean in-field firing rates of greater than 1.5 Hz, and had mean in-field firing rates more than three times larger than the mean out-of-field firing rate. Theta frequency was defined using the lag to the first peak in the autocorrelation of the LFP trace after band-pass filtering between 6 and 10 Hz using an FIR filter.

Phase precession was calculated as described[15]. Briefly, to assign a phase to a spike occurring at time $t$, we identified, in the filtered trace, the times of the theta peaks immediately preceding and following the spike ($t1$ and $t2$, respectively) and calculated the phase as $360(t-t1)/(t2-t1)$. We circularly shifted the phase of the spikes in 1° steps from 0° to 360°, continuing across the 360° border, and fit a linear regression line to the phase versus position plot at each rotation. We found the rotation with the best fit, such that the sum of squared errors between the fit line and data was minimized, and used the correlation coefficient between phase and position at this rotation as a measure of phase precession.

Computed fluorescence traces (**Supplementary Fig. 3**) were created by convolving a spike train with model fluorescence transients (rise time: $t1/2 = 52$ ms, decay time: $t1/2 = 384$ ms, peak amplitude taken from Figure 6c of ref. 13). All values in these traces below 10% $\Delta F/F$ were then set to 0 (**Supplementary Fig. 3**) to mimic the significant-transient-only traces generated for the real fluorescence time-series (**Fig. 2b**,**c**).


49. Pologruto, T.A., Sabatini, B.L. & Svoboda, K. ScanImage: flexible software for operating laser scanning microscopes. *Biomed. Eng. Online* **2**, 13 (2003).
50. Stosiek, C., Garaschuk, O., Holthoff, K. & Konnerth, A. In vivo two-photon calcium imaging of neuronal networks. *Proc. Natl. Acad. Sci. USA* **100**, 7319–7324 (2003).